Lunar Module Digital Autopilot

WILLIAM S. WIDNALL*
Intermetrics, Inc., Cambridge, Mass.

The lunar module digital autopilot is a first generation digital control system which would have been difficult to implement with conventional analog autopilot design techniques. The control synthesis problem was divided into the design of an attitude state estimator, the reaction-control-system (RCS) control laws, and the main engine thrust-vector control laws. The attitude state estimator derives the angular velocity and angular acceleration of the vehicle, based on measurements of vehicle attitude and assumed control response only. Rate gyros are not used. The RCS control laws employ parabolic switch curves in their phase plane logic to obtain fast response with a minimum of firings. The critical parameters are adapted in flight in response to varying flight conditions. An unconventional set of nonorthogonal axes is used to decouple the responses to RCS control about different spacecraft axes. A third-order minimum time control law is used to control the vehicle attitude by means of the thrusting descent engine. Performance in flight is presented.

Nomenclature

c = conversion factor having dimension of time
c_1,c_2,c_3 = constants for stored mass properties
CSM = command and service modules
F = thrust of the throttleable descent engine
I,I_q,I_r = moment of inertia about the Q or R axis
IMU = inertial measurement unit
K_ω,K_α = gains used in the state estimator
L = distance from descent engine gimbal plane to vehicle center of mass
LM = lunar module
m = spacecraft mass
$n,n-1$ = present, previous sample
n_p,n_u,n_v = number of RCS jets selected to torque about the P, U, and V axes
R = thrust vector actuator drive rate (0.2 deg/sec)
RCS = reaction control system
t = time at present sample instant
T = autopilot sample period (0.1 sec)
t_j = same as t_p, t_u, or t_v
t_p,t_u,t_v = jet torquing durations commanded by the P, U, and V RCS control laws—the sign gives the sign of the torque desired
u_q,u_r,u = thrust vector rotation command signal for the Q or R axis (1, 0, or -1)
u_{opt} = thrust vector rotation command signal for time-optimal control
v_e = assumed rocket exhaust velocity
x_1,x_2,x_3 = components of a nondimensional attitude state vector
α_j = magnitude of the angular acceleration that will result from firing the RCS jets for one axis
α_{pp} = magnitude of the P-axis angular acceleration that will result from firing one P-RCS jet
$\alpha_{qu},\alpha_{ru},\alpha_{u'u}$ = magnitudes of the Q, R, and U' components of angular acceleration that will result from firing one U-RCS jet
α_q,α_r,α = Q and R components of the estimated vehicle bias angular acceleration vector
$\dot{\alpha}_q,\dot{\alpha}_r,\dot{\alpha}$ = magnitude of the Q or R axis rate of change of angular acceleration that will result from commanding thrust vector rotation
δ = angle by which the U' and V' axes are skewed away from the U and V axes
$\delta\alpha,\delta\omega$ = correction to a component of the estimated angular acceleration, angular velocity, based on the unexplained attitude
$\Delta\alpha_q,\Delta\alpha_r$ = estimated changes in the Q and R bias angular accelerations due to thrust vector rotation commands in the last control interval
$\Delta\omega_p,\Delta\omega_q,\Delta\omega_r$ = estimated changes in the P, Q, and R angular velocities due to RCS jets commanded during the last control interval
$\Delta\theta_p,\Delta\theta_q,\Delta\theta_r$ = changes in P, Q, and R components of vehicle attitude (small angles)
Δt = sample period of the powered flight guidance equations (2 sec)
Δv = measured change in velocity due to thrusting
θ_e = attitude error
$\theta_o,\theta_i,\theta_m$ = outer, inner, and middle gimbal angles of the IMU
$\theta_{do},\theta_{di},\theta_{dm}$ = desired outer, inner, and middle gimbal angles
θ_{db} = attitude error deadband size in the RCS control laws
$\theta_p,\theta_q,\theta_r$ = P, Q, and R components of the unexplained attitude (small angles)
$\theta_{\max}$ = threshhold value that must be exceeded by a component of the unexplained attitude before an attitude measurement is incorporated
ω = estimated vehicle angular velocity vector
ω_d = desired angular velocity vector
ω_e = angular velocity error
$\omega_p,\omega_q,\omega_r$ = components of the estimated vehicle angular velocity

Received July 1, 1970; presented as Paper 70-991 at the AIAA Guidance Control and Flight Mechanics Conference, Santa Barbara, Calif. August 17-19, 1970; revision received October 8, 1970.

* Senior Engineer; formerly Director, Control and Flight Dynamics, Massachusetts Institute of Technology Instrumentation Laboratory, Cambridge, Mass.

Introduction

THE lunar module (LM) digital autopilot provides attitude control of the spacecraft during both coasting and powered flight. It is designed to control the three spacecraft configurations shown in Fig. 1: LM descent, LM ascent, and command and service modules (CSM) docked.

Torques for attitude control may be generated by the reaction control system (RCS) and by the descent propulsion system. The RCS employs 16 jets mounted in clusters of four on outriggers equally spaced around the LM ascent stage. Each jet has a thrust of 450 newtons. The descent propulsion system has a single engine that can be throttled from a maximum thrust of 45,000 newtons down to 12% of the maximum thrust. This engine is mounted in a gimbal system with actuators which can change the angle of the thrust vector relative to the spacecraft center of mass at the constant rate of 0.2 deg/sec. The ascent propulsion system has a single 16,000-newton engine, which is mounted rigidly

to the ascent stage. During ascent, attitude control must be maintained by use of the RCS jets alone.

The autopilot is an integral part of the LM primary navigation, guidance, and control system.[1,2] Most logical functions of this system are programed in the general purpose on-board digital computer, which has 36,864 words of fixed memory for program storage, and 2048 words of eraseable memory. The word length is 15 data bits plus a parity bit. It utilizes fixed decimal point arithmetic. The memory cycle time is 12 μsec. The execution of most instructions requires either two or three memory cycles.

The preliminary design of the autopilot is presented by Cherry and O'Connor.[3,4] A history of the development of the autopilot is presented by Cox.[5] This paper presents a summary of the final design of the autopilot as flown in the first lunar landing mission, Apollo 11. The complete design details are presented in Ref. 6.

Structure of the Autopilot

Three major subsections of the autopilot were identified, each of which could be designed somewhat independently: 1) the attitude state estimator, 2) the RCS control laws, and 3) the thrust vector control laws. The RCS control laws were divided into three separate channels, termed P, U, V. The locations and orientations of the RCS jets are such that if the spacecraft center of gravity lies near the geometric center of the 16 RCS jets (such as in the ascent configuration), then eight "P jets" thrusting only in the Y or Z directions produce torques about the P axis only (Fig. 2), four "U jets" thrusting in the $\pm X$ direction produce torques about the U axis only, and four "V jets" thrusting in the $\pm X$ direction produce torques about the V axis only.

The descent engine may be gimballed under computer control about the pitch (Q) axis and the roll (R) axis. Therefore, the descent-engine trim-gimbal control laws were separated into two channels (Q and R). The computation of the proper trim-gimbal drive for each channel is based on independent single-plane control laws.

The basic sample interval of the autopilot is 0.1 sec. Every 0.1 sec, whatever computer job is in progress is interrupted and control is transferred to the autopilot computations. Typically, it requires 0.025 sec to complete the autopilot computations. In addition to the main autopilot computations there is a subprogram that is executed every 2 sec in powered flight to adapt the autopilot gains as a function of the estimated decreasing vehicle mass and the estimated bias angular acceleration due to the thrusting main engine.

The most complex interaction between the guidance equations and the autopilot, and between subsections within the autopilot occurs during descent-engine powered flight (Fig. 3). The spacecraft velocity-changes due to thrusting are measured by the three integrating accelerometers of the inertial measurement unit (IMU). The velocity-change information is sampled every 2 sec by the computer and is used by the navigation equations to determine the present velocity and position. The guidance equations then compute the desired new thrusting attitude. In addition to commanding the desired thrusting attitude, the guidance equations can command changes in the thrust level of the throttleable descent engine.

The velocity-change information is also used every 2 sec (Δt) to update the estimates of spacecraft mass and thrust:

$$m(t) = m(t - \Delta t) - \Delta v\, m(t - \Delta t)/v_e \quad (1)$$

$$F = m(t)\Delta v/\Delta t \quad (2)$$

These estimates are inputs to the autopilot adaptive loop. The control effectiveness of the RCS jets about the P, Q, and R axes is calculated according to

$$\alpha_j = c_1 + c_2/(m + c_3) \quad (3)$$

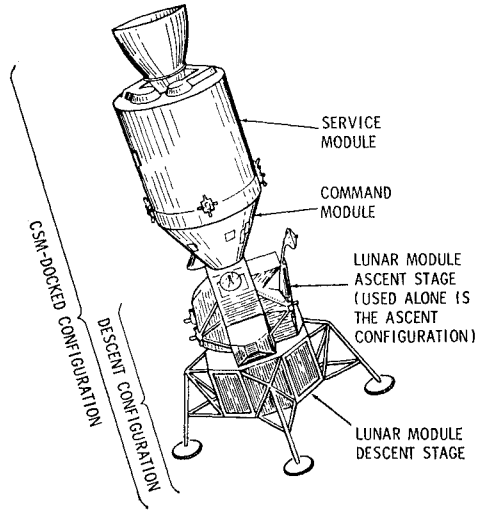

Fig. 1 Spacecraft configurations controlled by the lunar module autopilot.

A separate set of constants is appropriate for each axis and for the descent and ascent configurations. The values so calculated for the orthogonal angular acceleration components α_{qu} and α_{ru} are then resolved onto the U' axis to determine $\alpha_{u'u}$. Because of the inertia symmetry, the value of $\alpha_{u'u}$ can be used also for V axis computations.

The effectiveness of the thrust-vector control signals in the descent configuration is calculated according to

$$\dot{\alpha}_q = FLR/I_q, \quad \dot{\alpha}_r = FLR/I_r \quad (4)$$

where F is calculated by Eq. (2), I_q and I_r are calculated as being inversely proportional to α_{qu} and α_{ru}, and L is calculated as

$$L = c_4 + c_5/(m + c_6) \quad (5)$$

Attitude State Estimator[6]

The basic measurements of the vehicle attitude state available to the autopilot are the gimbal angles of the inertial measurement unit, which are sampled every 0.1 sec. To separate any bias angular acceleration due to the main engine

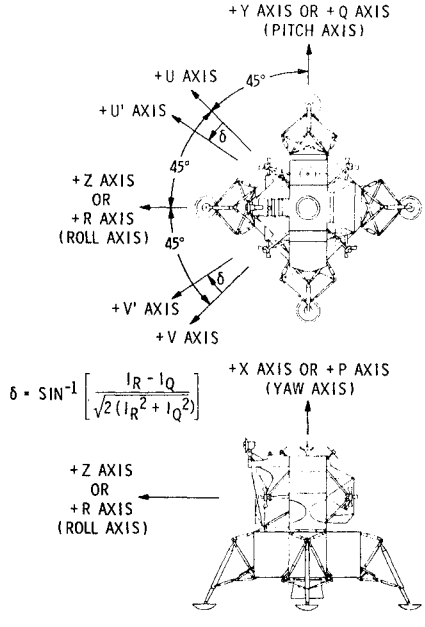

Fig. 2 The control axes of the LM.

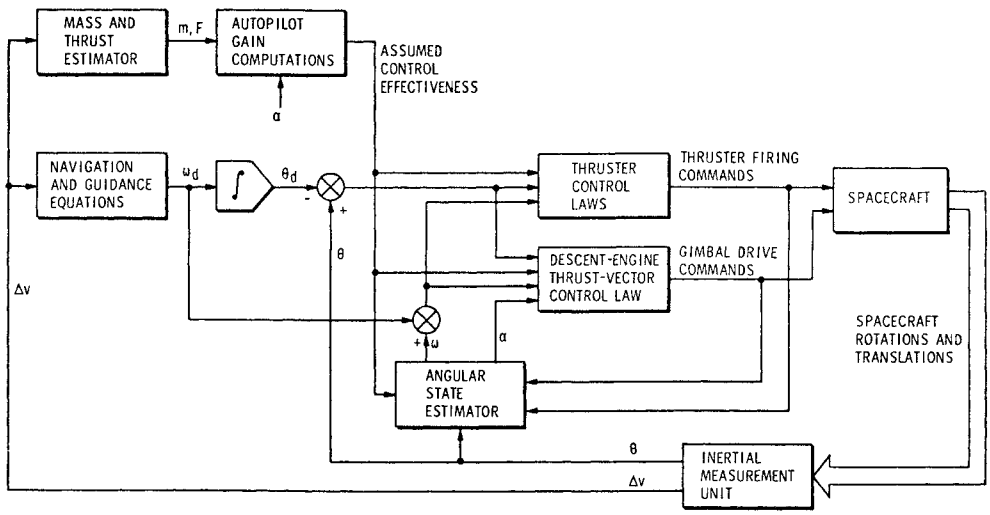

Fig. 3 Information flow in the autopilot during descent-engine powered flight.

from the angular acceleration due to RCS jet firings, the state estimator needs additional inputs from the RCS control laws containing the jet-firing information. Including jet-firing information as well as thrust-vector-command information gives an added benefit; the basic attitude inputs may be filtered as required, without necessarily introducing large lags into the estimates of angular velocity and bias angular acceleration.

The estimated changes in the P, Q, and R angular velocities due to RCS jets selected during the last control interval are computed as

$$\begin{aligned} \Delta\omega_p &= \alpha_{pp} t_p n_p \\ \Delta\omega_q &= \alpha_{qu}(t_u n_u - t_v n_v) \\ \Delta\omega_r &= \alpha_{ru}(t_u n_u + t_v n_v) \end{aligned} \tag{6}$$

The estimated changes in the Q and R bias angular acceleration due to thrust vector rotation commands in the last control interval are computed as

$$\Delta\alpha_q = \dot{\alpha}_q T u_q, \quad \Delta\alpha_r = \dot{\alpha}_r T u_r \tag{7}$$

The IMU gimbal angles observed during the previous execution of the estimator computations have been stored. The present gimbal angles are now sampled, the change in gimbal angles is computed, and the change is transformed to a change in body angles. The difference between the measured change in attitude and the predicted change in attitude is called the unexplained change in attitude. This is computed and added to the previous total unexplained attitude to form the present total unexplained attitude:

$$\theta_p(n) = \theta_p(n-1) + \Delta\theta_p - [\omega_p(n-1)T + \Delta\omega_p T/2] \tag{8a}$$

$$\theta_q(n) = \theta_q(n-1) + \Delta\theta_q - [\omega_q(n-1)T + \alpha_q(n-1)T^2/2 + \Delta\omega_q T/2] \tag{8b}$$

$$\theta_r(n) = \theta_r(n-1) + \Delta\theta_r - [\omega_r(n-1)T + \alpha_r(n-1)T^2/2 + \Delta\omega_r T/2] \tag{8c}$$

The quantities in brackets may be identified as components of the predicted attitude change. Note that the predicted attitude change due to gimbal drive commands has been neglected, and the exact expression for the attitude change due to jet firings has been approximated by a simpler term.

The unexplained attitude is used to update the estimates of angular velocity and angular acceleration. But first, logic is applied to reject the measurement quantization noise. Since the probability distribution of this noise is not Gaussian but is rectangular, the noise may be largely rejected by a nonlinear filter logic which is applied independently to the P, Q, and R axes in the state estimator. For each axis, if the component of the unexplained attitude is less than a threshold value $\theta_{max} = 0.14$ deg, then the unexplained attitude is assumed to be largely due to the attitude measurement quantization noise. In this case, the corrections $\delta\omega$ and $\delta\alpha$ to the estimates of angular velocity and bias angular acceleration for that axis are set to zero. The unexplained attitude is *not* zeroed. However, for each axis where the unexplained attitude exceeds the threshold, it is assumed that the estimated angular velocity and angular acceleration for that axis are in need of corrections. Nonzero corrections $\delta\omega$ and $\delta\alpha$ are computed as

$$\delta\omega = K_\omega\theta(n)/T, \quad \delta\alpha = K_\alpha\theta(n)/T^2 \tag{9}$$

and then the unexplained attitude $\theta(n)$ for that axis is reset to zero.

The estimates of the angular velocity and the bias angular acceleration are now updated to the present sample instant as

$$\omega_p(n) = \omega_p(n-1) + \Delta\omega_p + \delta\omega_p \tag{10a}$$

$$\omega_q(n) = \omega_q(n-1) + \alpha_q(n-1)T + \Delta\omega_q + \delta\omega_q \tag{10b}$$

$$\omega_r(n) = \omega_r(n-1) + \alpha_r(n-1)T + \Delta\omega_r + \delta\omega_r \tag{10c}$$

$$\alpha_q(n) = \alpha_q(n-1) + \Delta\alpha_q + \delta\alpha_q \tag{11a}$$

$$\alpha_r(n) = \alpha_r(n-1) + \Delta\alpha_r + \delta\alpha_r \tag{11b}$$

Note that bias angular acceleration about the P axis is assumed to be zero, and the estimated rate-change term due to trim-gimbal activity in the last control interval has been neglected. In periods of coasting flight, it is assumed that the Q and R components of bias angular acceleration are also zero. Accordingly, the final step in the state estimator sets α_q and α_r to zero during periods of coasting flight.

The dynamic characteristics of the state estimator are strongly determined by the choice of filter gains K_ω and K_α. The gains selected[6] were a compromise between fast estimation response and rejection of bending mode and propellant slosh oscillations. Extensive simulations were used to demonstrate satisfactory estimator performance.

RCS Control Laws[6]

Within the computational capacity of the LM guidance computer, the fastest repetition rate that is possible for the autopilot calculations is 10 cps. However, in the lightest ascent configuration, two RCS jets torquing can produce an angular acceleration of about 50 deg/sec^2. The simplest form of RCS control law would turn-on and turn-off the RCS jets only at the control sample instants. However, if this approach were used, the angular velocity of the lightest ascent configuration would be controlled to an accuracy of only 5 deg/sec. This is clearly unacceptable. To overcome this difficulty, the assumed control effectiveness of the RCS jets is used to determine the exact jet firing durations that are required to deliver a desired change in angular velocity.[3,4]

For automatic control in the LM-alone case, a subroutine is programed which calculates the required jet torquing time t_j for one axis as a function of: 1) the attitude error θ_e and the angular velocity error ω_e, 2) the parameters, as calculated in the adaptive loop, that determine the curvature and position of phase plane parabolas, and 3) the preference for 1-jet or 2-jet firings to obtain the required torque impulse. By successive calls to this subroutine, with the appropriate input information for each axis, the jet firing times for each axis are determined.

The control logic applied by the subroutine in coasting flight is illustrated by the phase plane diagram shown in Fig. 4. The phase plane above the θ_e axis is divided into five zones. The boundaries of these zones are parabolas. The steepness of the parabolas bounding zone 2 are identical to that of the estimated vehicle phase plane trajectory when the jets are torquing. The jet acceleration magnitude which determines this parabola was calculated in the adaptive loop. The parabola separating zone 4 and zone 5 is *not* a trajectory of the vehicle. It is flat to keep control angular velocities low, but is not so flat that a large θ_e can persist. The parabolic form is retained to keep the boundary logic general for compactness of coding. The flatness selected corresponds to an acceleration of 1.4 deg/sec^2. A smaller acceleration could not have been chosen without rescaling the fixed-point arithmetic calculations. The intercepts of the parabolas with the θ_e axis are a function of the deadband θ_{db} selected by the astronaut or by the automatic maneuver program. Available attitude error deadbands are 0.3, 1.0, and 5.0 deg.

This phase plane design is such that the control action in response to any initial condition will transfer the state toward the origin with at most two major pulses. This is illustrated by segment A-B-C of the sample trajectory in Fig. 4. After the acquisition of the deadzone, the vehicle state is held in a minimum impulse limit cycle, as shown by segment D-E-F-G.

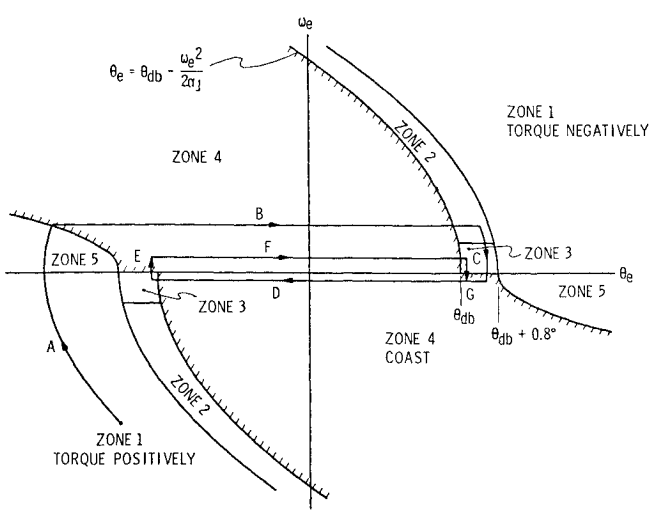

Fig. 4 RCS control law for LM-alone coasting flight.

The state traverses the deadzone, and its direction is reversed by a single firing of one RCS jet each time a zone 3 is encountered.

The control logic applied by the subroutine in powered flight is illustrated by the phase plane diagram shown in Fig. 5. The intercepts of the various parabolas are shifted as a function of the magnitude of the estimated bias angular acceleration. The intercept locations shown in Fig. 5 are typical for powered ascent with a large ascent engine thrust vector misalignment. The steepness of the four parabolas are based on four different angular accelerations. The upper left parabola is based on the minimum acceleration $\alpha_{min} = 1.4$ deg/sec^2 as in coasting flight. The upper right parabola is based on the net acceleration possible with the jets firing against the bias torque. The lower right parabola is based on the bias angular acceleration alone (no jets firing), however, it is steepened by a factor $\frac{9}{8}$ to improve the probability that the trajectory would not recross the switch curve into the torquing zone causing an unnecessary small pulse.

A typical phase plane trajectory is shown superimposed on the phase plane logic in Fig. 5. The phase plane design is such that the vehicle is controlled with a low-frequency limit cycle in which the jets are commanded to fire a single pulse in opposition to the bias torque once each cycle.

The autopilot must perform the same basic control functions in the CSM-docked case as in the LM-alone case. However, a separate subroutine was developed for the CSM-docked case.[6] A problem peculiar to the docked configuration is that the vehicle has three low-frequency bending modes associated with the relatively weak docking adapter connecting the vehicles. To guarantee that the RCS jets could not be fired at the bending frequency, jet inhibition logic[7] was designed for the CSM-docked case.

In addition to the RCS control laws provided to follow the automatic attitude commands, separate control laws are provided to follow manual attitude commands, as inputed to the computer by the rotational hand controller.[8]

An interesting performance problem existed with an earlier autopilot design, in which the orthogonal *P-U-V* axes were used for the application of the single-axis phase-plane RCS control laws. Figure 6[9] shows the *U*-axis jet firings as telemetered to the ground during a short portion of ascent-stage-only powered flight in Apollo 9. One can see evidence of the low-frequency limit cycle, in agreement with the design intent, in which the bias torque from the thrusting ascent engine is balanced by torque pulses from one *U*-axis jet. (The *U*-axis jet selected is the one that can provide the desired sign torque by thrusting in the same direction as the ascent engine.) However, note in addition to the four substantial RCS pulses there are five useless small pulses.

These multiple jet firings are caused by inertia cross-coupling effects. The mass distribution in the LM is such that the principal axes of the moment of inertia are aligned closely with the *Q* and *R* axes, not the *U* and *V* axes. As a re-

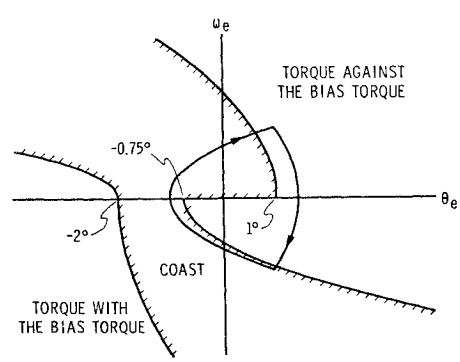

Fig. 5 RCS control law for LM-alone powered flight with a large bias torque.

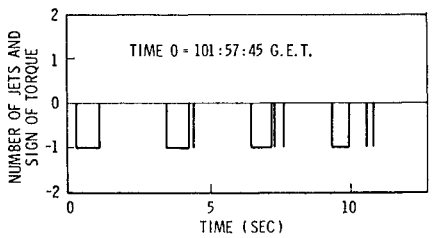

Fig. 6 Typical U-axis jet firings during Apollo 9 ascent powered flight.

sult, applying a torque with a V-axis jet produces an angular acceleration not only along the V axis but also along the U axis. The magnitude of this cross-coupled acceleration is such that in the worst case the angular acceleration vector is about 15° away from the applied torque vector. During the same interval of time shown in Fig. 6 a similar low-frequency limit cycle existed about the V axis. The V-axis pulses were occurring slightly delayed with respect to the U-axis major pulses. Hence at the end of a major U-axis pulse, the V-axis jet was still firing. This V-axis torque produced a cross-coupled angular acceleration along the U axis. This in turn caused the U-axis phase-plane trajectory to leave the coast zone and return to the torquing zone. The result is unwanted small pulses. This cross-coupling effect had been anticipated before flight as a result of detailed autopilot performance simulations.[10,11]

To decouple the RCS control channels and thereby reduce the number of RCS firings, a nonorthogonal set of control axes called U' and V' was introduced.[12] The U' and V' axis directions are uniquely determined by the requirement that the U' direction shall be orthogonal to the angular acceleration induced by applying either a V-axis torque or a P-axis torque, and the V' direction shall be orthogonal to the angular acceleration induced by applying either a U-axis torque or a P-axis torque. The U' and V' axes are skewed symmetrically with respect to the LM R axis as shown in Fig. 2. The sines and cosines of the angle δ, by which the U' and V' axes are skewed away from the U and V axes toward the R axis, are

$$\sin\delta = (I_r - I_q)/[2(I_r^2 + I_q^2)]^{1/2} \tag{12a}$$

$$\cos\delta = (I_r + I_q)/[2(I_r^2 + I_q^2)]^{1/2} \tag{12b}$$

By resolving the attitude error vector and the angular velocity error vector onto the U' and V' axes and by utilizing the U' and V' components for the purpose of determining U and V jet torquing requirements, the two control channels have been decoupled.

Thrust-Vector Control Laws[6,14]

It was the intent of the spacecraft designers that the gimballing capability of the descent engine would be used to place the thrust vector through the spacecraft center-of-mass. This would eliminate any torque on the vehicle due to the descent-engine thrust and thereby reduce the propellant expenditure rate of the RCS jets. Since attitude control would be maintained by the RCS jets, there was no design requirement to provide a high-speed engine-gimballing capability for thrust-vector control. Therefore, light-weight, low-power actuators were selected. These were geared so that the engine angle could be commanded to change at only 0.2 deg/sec. The actuator interface with the computer is simply an on-off interface. For both the Q axis and the R axis about which the thrust direction can be controlled, the computer can command a positive drive rate (+0.2 deg/sec), a negative drive rate (−0.2 deg/sec), or zero drive rate.

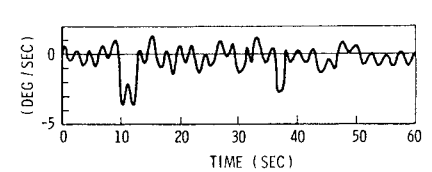

Fig. 7 Pitch-rate during a portion of the lunar landing powered descent.

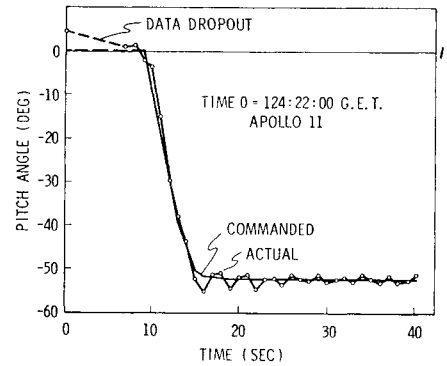

Fig. 8 Pitch guidance command and response, initial phase of powered ascent.

However, minimizing the propellant expenditure of the RCS jets was an essential design consideration. It was noted that torques for attitude control could be developed without a propellant-expenditure penalty by using the descent engine, because the descent engine in powered flight would be firing continuously. Therefore, an attitude control law was sought that would utilize the descent engine in such a way as to permit attitude control without the assistance of the U-V axis RCS thrusters. The control law selected was the one which would provide the fastest possible response time—that is, the minimum-time control law.

About either the Q axis or the R axis, the differential equation relating the gimbal-drive control signal to the deviation of the vehicle attitude away from the desired attitude is

$$d^3\theta_e/dt^3 = \dot{\alpha}u \tag{13}$$

where $\dot{\alpha}$ is given in Eq. (4).

The first and second derivatives of the attitude error are the angular velocity error and the angular acceleration error. Assuming that these state variables are all provided to the control law with no measurement noise or estimation error, the optimal control may be determined as a function of the present state by the following sequence of calculations:[13,14]

$$c = (\dot{\alpha})^{-1/3}$$

$$x_1 = c^2\alpha_e,\ x_2 = c\omega_e,\ x_3 = \theta_e,\ s_1 = \text{sign}(x_1) \tag{14}$$

$$s_2 = \text{sign}(x_2 + s_1x_1^2/2)$$

$$u_{\text{opt}} = -\text{sign}[x_3 + x_1^3/3 + s_2x_1x_2 + s_2(s_2x_2 + x_1^2/2)^{3/2}]$$

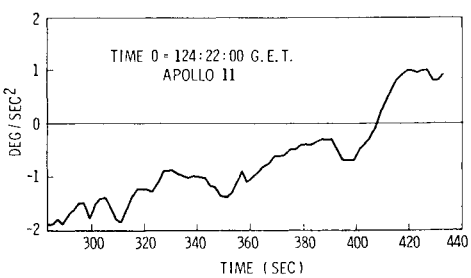

Fig. 9 V'—component of estimated bias angular acceleration during final phase of powered ascent.

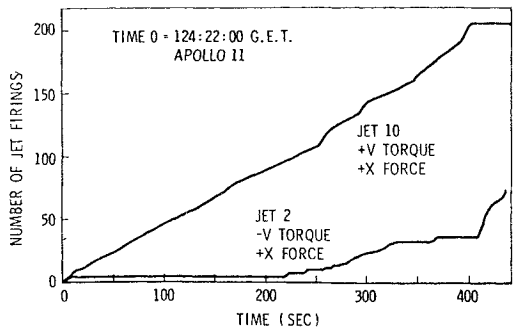

Fig. 10 Total V-axis RCS jet firings during powered ascent.

The parameter c has the dimension of time and converts the state $(\alpha_e,\omega_e,\theta_e)$ into a nondimensional state (x_1,x_2,x_3). The optimal control signal u_{opt} is then given in terms of the nondimensional state.

Performance during the First Lunar Landing

The LM autopilot has flown with dramatic success in the several Apollo missions, including the lunar landings. Telemetered data plus comments from the astronauts confirm that the autopilot performs in flight in close agreement with the intended performance.

During the first lunar landing (Apollo 11) the autopilot followed first the automatic and later the manual attitude commands, changing from a nearly horizontal thrusting attitude at ignition to a vertical (upright) attitude at touchdown. During the first four minutes of the powered descent after the initial transient, the thrust-vector attitude control law was successful at following the slowly changing attitude commands without the assistance of the U or V RCS jets. Later, a propellant slosh oscillation developed with amplitude sufficiently large to exceed the deadbands in the RCS control laws. Small RCS firings were commanded to limit the slosh oscillation amplitude. The slosh oscillation at 0.5 Hz may be seen in the pitch angular velocity shown in Fig. 7.[9] The automatic guidance was landing the spacecraft among numerous boulders, so Armstrong switched from automatic to manual attitude commands and pitched the Eagle upright to extend the trajectory beyond the rock field.[15]

The pitch attitude following liftoff from the lunar surface is shown in Fig. 8.[9] After 10 sec of vertical rise, the automatic guidance commanded a pitch-over of 50 deg at a rate of 10 deg/sec. Note the rapid response provided by the RCS control laws. The actual attitude follows closely the desired attitude. After the pitch-over maneuver, the typical ascent low-frequency attitude limit cycle can be seen.

As the ascent propellant is expended, the center of mass moves from behind the thrust vector ($-Z$ direction) at liftoff to slightly ahead of the thrust vector ($+Z$ direction) at cutoff. This causes a time-variation in the bias angular acceleration components along both the U' and V' axes. The V' component of the bias angular acceleration as computed by the state estimator during the last 150 sec of powered ascent is shown in Fig. 9.[9] The autopilot adapted its critical parameters in the RCS control laws in response to this varying estimated bias acceleration. The accumulated number of firings of the V axis RCS jets for the entire powered ascent is shown in Fig. 10 (Ref. 16). After liftoff and the initial pitchover, it is evident that attitude control about the V axis was maintained for about 200 sec by firing the $+V$ jet only. Later the limit cycle amplitude increased until firings from both the $+V$ jet and the $-V$ jet were required to maintain attitude control. Although the $-V$ torque firings produce angular acceleration in the same direction as the bias angular acceleration of the ascent engine, nevertheless both the $+V$ torque and $-V$ torque are generated by upward forcing ($+X$) jets and hence, represent no loss in Δv. This period of $+V$ and $-V$ torquing may be related to propellant slosh oscillations.[16] Near the end of the powered ascent after the bias angular acceleration has reversed sign, no further firings are commanded of the $+V$ jet and attitude control is maintained about the V axis by the $-V$ jet alone. With the nonorthogonal control axes, no unnecessary small pulses were seen.

Conclusions

The autopilot synthesis problem was divided into three subproblems: the design of an attitude state estimator, the design of RCS control laws, and the design of the thrust-vector control laws. The control laws were further subdivided into separate channels. The axes chosen for application of the separate RCS control laws were nonorthogonal. This design effectively eliminated performance problems that existed because the torque vectors of the RCS jets were not parallel to the principal axes of inertia of the vehicle.

The attitude state estimator computes the angular velocity and angular acceleration of the vehicle, based on measurement of vehicle attitude and assumed control response. The success of this state estimator demonstrates that rate gyros are not required sensors for an autopilot. They may be eliminated to achieve an increase in over-all system reliability.

The RCS control laws in the LM-alone case employ parabolic switch curves in their phase plane logic. The critical parameters in the RCS control laws are adapted in response to the varying mass of the spacecraft and the bias angular acceleration due to the thrusting main engine. The control law design permits rapid response to commands with a minimum of jet firings. Satisfactory control is possible even in the lightest ascent configuration because the RCS control laws compute the exact firing time required to achieve a desired rate change.

A third-order minimum time control law is used to control the vehicle attitude by means of the thrusting descent engine. This permits attitude control often without the assistance of the RCS jets.

References

[1] Miller, J. E. ed., *Space Navigation Guidance and Control*, AGARDograph 105, 1966, Technivision Ltd., Maidenhead, England.

[2] Hoag, D. G., "Apollo Navigation, Guidance, and Control Systems: A Progress Report," April 1969, National Space Meeting of the Institute of Navigation, Houston, Texas.

[3] Cherry, G. W. and O'Connor, J., "Design Principles of the Lunar Excursion Module Digital Autopilot," R-499, July 1965, M.I.T. Instrumentation Lab., Cambridge, Mass.

[4] Cherry, G. W., "Design Principles for an Integrated Guidance and Control System for the Lunar Excursion Module," AIAA Fourth Manned Space Flight Meeting, Oct. 1965, St. Louis, Mo.

[5] Cox, K. J., "A Case Study of the Apollo Lunar Module Digital Autopilot," IEEE Case Studies in System Control, 69-C41-AC, Aug. 1969, Boulder, Colo.

[6] Widnall, W. S. et al., "Digital Autopilot," Sec. 3 (Rev. 1) of "Guidance System Operations Plan for Manned LM Earth Orbital and Lunar Missions Using Program LUMINARY 1A," R-567, June 1969, M.I.T. Instrumentation Lab., Cambridge, Mass.

[7] Kalan, G. R., "Improvement of the Bending Stability of the LM Autopilot in the CSM-Docked Configuration," SAD 18-69, April 1969, M.I.T. Instrumentation Lab., Cambridge, Mass.

[8] Stengel, R. F., "Manual Attitude Control of the Lunar Module," *Journal of Spacecraft and Rockets*, Vol. 7, No. 8, Aug. 1970, pp. 941–948.

[9] Delashmit, W. H. and Lee, R., "Apollo DAP Postflight Analysis Summary," EG-70-10, March 1970, NASA/MSC, Houston, Texas.

[10] Croston, R. C., Raney, J. L., and Goeckler, W. B., "Digital Autopilot for the LM Mission Simulator," IAF Congress, Oct. 1968, New York.

[11] Widnall, W. S. et al., "LM Digital Autopilot Simulation Results Using Program SUNDANCE," E-2377, Jan. 1969, M.I.T. Instrumentation Lab., Cambridge, Mass.

[12] Goss, R. D., "Nonorthogonal Axis System for LM Digital Autopilot," SAD 12-69, March 1969, M.I.T. Instrumentation Lab., Cambridge, Mass.

[13] Widnall, W. S., "Derivation of the Optimum Control Program for Steering the LEM Using the Gimballed Descent Engine," SGA 3-66, Jan. 1966, M.I.T. Instrumentation Lab., Cambridge, Mass.

[14] Widnall, W. S., "The Minimum-Time Thrust-Vector Control Law in the Apollo Lunar-Module Autopilot," *Automatica*, Vol. 6, No. 5, Sept. 1970, pp. 661–672.

[15] Stengel, R. F., "The Manually-Controlled Landing of Eagle," SAD 28-69, Aug. 1969, M.I.T. Instrumentation Lab., Cambridge, Mass.

[16] Goss, R. D., Private communication, Sept. 23, 1969, M.I.T. Instrumentation Lab., Cambridge, Mass.